Stony Brook University

The Microstructure and Properties of Plasma Sprayed Ceramic Composites

A Thesis Presented

by

Kerry James LaPierre

to

The Graduate School

in Partial Fulfillment of the

Requirements

for the Degree of

Master of Science

in

Materials Science and Engineering

Stony Brook University

December 2010

Stony Brook University

The Graduate School

Kerry James LaPierre

We the thesis committee for the above candidate for the
Master of Science degree hereby recommend acceptance of this thesis

Sanjay Sampath – Thesis Advisor
Professor, Department of Materials Science & Engineering

Herbert Herman
Professor Emeritus, Department of Materials Science & Engineering

Albert Tobin
Adjunct Professor, Department of Materials Science & Engineering

This thesis is accepted by the Graduate School

Lawrence Martin

Dean of Graduate School

Abstract of the Thesis

The Microstructure and Properties of Plasma Sprayed Ceramic Composites

by

Kerry James LaPierre

Master of Science

in

Materials Science and Engineering

Stony Brook University

2010

The microstructure and properties of plasma-sprayed ceramics and ceramic matrix composites (CMCs) have been investigated. Substrate-free deposits were fabricated by plasma spraying onto expendable graphite substrates. The deposits were evaluated in the as-sprayed and heat-treated conditions. X-ray diffractometry (XRD) was used in conjunction with differential scanning calorimetry (DSC) to examine the phase content and transformation temperatures of plasma-sprayed Al_2O_3. Mechanical properties were measured using three-point flexural testing and density measurements were made for both the as-sprayed and heat treated conditions. Significant increases in modulus and strength were achieved as a result of post -spray heat treatment.

Having established baseline properties with respect to the pure matrix material, the effect of incorporating a second phase was examined. Ceramic matrix composites were fabricated by plasma-spraying a mechanical mixture of Al_2O_3 and SiC particulate. Composites consisted of particulate SiC and re-solidified inclusions in an Al_2O_3 matrix. Significant improvements in strength and modulus resulted from the incorporation of second phase combined with heat-treatment

Dedicated to my Mother and Father

Table of Contents

List of Figures

List of Tables

Acknowledgments

The author wishes to express his sincere gratitude to Dr. Herbert Herman and Dr. Sanjay Sampath whose positive contribution extends well beyond this study.

The author would also like to thank Dr. Albert Tobin for sharing his knowledge and friendship.

A significant contribution was made by my friends and colleagues at the Thermal Spay Laboratory including Glenn Bancke, Rajesh Tiwari, Yvonne Huran, and Robert Greenlaw.

Special thanks are due Dr. Philip Adler, Herbert Baker, Garret Bush, Dr. John Papazian, Dr. William Rooney, and Theotis Williams of the Grumman Corporate Research Center for contributing their expertise, time, and facilities to this effort.

1. INTRODUCTION

1.1 Plasma Spray Processing

Plasma spraying is an established technique for the deposition of coatings. Applications include ceramic thermal barrier coatings for gas turbine engine components, reclamation of worn parts, and the processing of high T_c ceramic superconductors.

The basic plasma gun utilized in plasma spraying in atmosphere (APS) consists of a water cooled anode which serves as a nozzle and a conical tungsten cathode (Figure 1). The cathode is thoriated to reduce the electron work function and thus provide a more stable arc. A steady flow of inert gas, usually argon, is maintained within the cathode - anode space and exits the gun through the annular nozzle.

An electrical discharge initiated between the positive and negative electrodes serves to ionize the gas. As ions and electrons are accelerated towards their respective electrodes they collide with neutral gas atoms to create an avalanche effect. The net result is an electrically neutral gaseous collection of energetic electrons and ions; a plasma.

As the plasma exits the nozzle, the exothermic recombination of electrons and ions generates temperatures in excess of 15,000 ºC. In addition to the primary plasma gas, a diatomic secondary gas is often added to increase the enthalpy content of the plasma flame.

A particulate ceramic or metal, carried by means of an inert gas stream, is generally introduced into the plasma flame as it exits the nozzle, wherein it is melted and accelerated to velocities approaching that of sound. Upon impact with the substrate these molten particles "splat" to assume a tortuous yet generally platelet-like shape (Figure 2). Rapid solidification occurs to produce sub-micron grain size and, in some cases, amorphous structure. As particles rain down, typically at rates of 10^6 m^{-2}/s [1], a dense coating is built up having the lamellar microstructure characteristic of plasma spray processing.

Defects observed in plasma sprayed deposits include porosity, un-melted, and re-solidified particles. In general these defects are deleterious to coating integrity and are minimized through optimization of processing parameters which include particle size, arc power, and spray distance.

Although plasma spraying has traditionally been applied to the deposition of coatings, it has also been used for the fabrication of free-standing articles. Missile nose cones[1] and radomes[2] have been manufactured by plasma spraying onto and subsequent removal from an appropriate form. For form removal Holcombe and Powell[3] utilized thermal expansion mismatch between the substrate and coating to produce substrate-free ceramic articles. Holcombe[4] later reported the use of graphite mandrels which were removed by heating in an oxidizing atmosphere. This latter technique is especially promising since it should be applicable to any geometry which can be plasma sprayed.

More recently, Schindler and Schultz[5] have plasma sprayed rotationally symmetric, free-standing ceramics with diameters of up to 0.5 m and thicknesses approaching 3 mm. These components were generated by spraying a pure oxide ceramic onto a rotating metal mandrel. Form removal was accomplished through immersion in liquid nitrogen. Excellent machinability was reported, and no deleterious effects were observed as a result of the transformation of metastable γ-Al_2O_3 to the equilibrium corundum structure during heat treatment.

1.2 Ceramic-Matrix Composites

The severe operating conditions of oxidation and elevated temperatures to be encountered by advanced aircraft have precluded the use of traditional metals and alloys. A need exists for strong, lightweight, durable materials capable of filling this gap.

The low density, high stiffness, and excellent thermal properties of ceramics suggest a natural alternative to metals. Unfortunately, the general inability of ceramics to undergo plastic deformation and the resultant brittleness has severely limited their use in structural applications.

Improved modulus, strength, and fracture toughness have been achieved through the incorporation of fibers and whiskers in ceramic matrices. Marshal and Ritter [6] have reviewed strengthening and toughening mechanisms in ceramic-matrix composites (CMCs). It is found that the nature of the fiber-matrix interface is of principal importance in determining composite properties.

In addition to increased strength and fracture toughness, Al_2O_3-SiC whisker composites are very resistant to slow crack growth[7], thermal shock[8], and high temperature creep[9, 10].

Numerous studies have been conducted to determine the effect of various processing routes on ceramic-ceramic composite properties. In the case of a discontinuous reinforcing phase, a three-step process is generally followed which entails mixing of the constituents, shape forming, and densification.

Suspension routes, including electrostatic repulsion[11] and the use of polymeric dispersants[12], are often used to achieve homogeneous mixing of the matrix and reinforcement.

Shape forming operations are generally carried out by compaction of the dried mixtures. Exceptions include the use of press filtration[10] and slip-casting[13] to obtain dense green bodies.

Densification during sintering is inhibited due to shrinkage incompatibilities between the matrix and dispersed phases[14,15]. This difficulty has been overcome to some extent by the presence of a reactive liquid phase during sintering[12,16,17].

Optimum properties have been achieved by hot isostatic-pressing[10,11,18,19]. Unfortunately this process is prohibitively expensive and imposes severe limitations on the size and shape of the final product.

1.3 Plasma Spray Processing of Ceramic-Matrix Composites

Plasma spray processing lends itself nicely to the fabrication of ceramic composites. It is applicable to a wide range of materials. The only requirement is that the material to be sprayed does not decompose, sublime, or otherwise react in the plasma flame. Near net shapes can be achieved by spraying directly on a substrate in the shape of the desired part.

Easy variation in the relative fractions of the matrix and reinforcing phases is possible. Either a simple feed of blended powders or dual feed, where each component is fed separately and undergoes mixing in the plasma flame, may be employed.

The latter process offers the ability to fabricate graded deposits[20]. In the case of a reinforcing material that is unstable in the plasma flame or when melting is otherwise undesirable, dual feed enables "downwind" injection into a cooler region of the plasma flame whilst the matrix material undergoes complete melting through standard injection.

Plasma spraying is the prevalent method for the generation of cermet[21] and particulate CMC[20] coatings. Iwamoto et al[22] have produced whisker-reinforced Al_2O_3 coatings by plasma spraying. It is inferred that these coatings were produced by spraying a mechanical mixture of alumina + whiskers. Mechanical property tests were carried out on 1.5% and 3.0% (weight) loadings for both SiC and Si_3N_4 whiskers. It was reported that whisker-reinforced coatings showed greatly improved thermal shock resistance and coating-

substrate adhesion. Berndt and Yi [23] fabricated both metal and ceramic matrix whisker-reinforced coatings. Difficulties encountered in the feed of whiskers and melting of whiskers within the flame were overcome to some extent by the fabrication of agglomerated powders and careful selection of spray parameters.

1.4 Mechanical Properties of Plasma-Sprayed Ceramics

Limited data exists on the mechanical properties of plasma-sprayed ceramics: Berndt[24] utilized tensile adhesion testing to investigate the properties of NiCrAlY and NiCrAlZr + ZrO_2 -Y_20_3 (8 wt. %) coating systems. A compliance calibration was carried out to account for deformation in the specimen fixture enabling the stress-extension behavior of the coating system to be described.

Steffens and Fisher[25] examined Young's modulus and compressive strength as a function of porosity in plasma sprayed ZrO_2 Free-standing tubes were prepared by plasma spraying onto rotating metal tubes which were subsequently dissolved.

Boch et al [26] examined variations in the elastic modulus associated with structural phase transformations in plasma-sprayed Al_2O_3. Studies were carried out at temperature using vibrating plate and ultrasonic techniques.

Siemers and Mehan [27] utilized 4-point flexural testing in conjunction with acoustic emission to examine the properties of MgO and Y_2O_3 stabilized ZrO_2. Properties were evaluated for both the substrate-free condition and as-bonded to

a metal substrate.

Although different materials, fabrication techniques, and test methods make correlation of results difficult, it was generally observed that the elastic moduli of plasma sprayed-ceramics are almost an order of magnitude lower than their monolithic counterparts.

To the knowledge of this investigator no such studies have been directed towards the properties of substrate-free plasma-sprayed ceramic matrix composites.

2. STATEMENT OF THE PROBLEM

Greater use of plasma spraying as a means of fabricating free-standing ceramic articles will require a better understanding of, and, an ability to improve the properties of plasma-sprayed ceramics.

A comprehensive study was undertaken to investigate the effect of heat treatment and second phase incorporation on the microstructure and properties of plasma-sprayed ceramics.

Differential scanning calorimetry (DSC) was used in conjunction with x-ray diffractometry (XRD) to examine the transformation temperatures, phase content, and enthalpies associated with the reconversion of plasma sprayed Al_2O_3. Heat treatments were conducted to isolate particular events during the microstructural evolution and their effect on the properties of sprayed deposits was then examined. Density measurements were made utilizing Archimedes' Principle with water as the immersion medium. Mechanical attributes were examined using three-point bend testing for both the as-sprayed and heat treated conditions. Results are examined in light of previous work

Having established baseline properties with respect to the pure matrix material, the effect of incorporating a second phase was examined. Ceramic matrix composites were fabricated by plasma-spraying a mechanical mixture of Al_2O_3 and particulate SiC. Properties were re-evaluated under identical conditions. Particular emphasis was placed on characterizing the microstructure of these composites.

3. EXPERIMENTAL

3.1 Specimen Fabrication

A Metco 3MB* hand-held plasma spray gun was used in the course of this study. Spray parameters (Table 1) were optimized for the feedstock: a 53 µm (nominal size) aluminum oxide†

Substrate-free deposits were prepared by plasma spraying onto the 2.5cm x 7.5cm face of 2.5cm x 7.5cm x 18cm graphite‡ mandrels. Suitable adhesion was obtained by roughening the graphite surface with 180 grit abrasive paper. Sharp edges were chamfered to minimize residual stresses at the edge of specimens. Specimens were typically sprayed to a thickness of 0.09cm (0.035 in) and removed from the block by use of an abrasive cut-off wheel. Approximately 1 mm of graphite, left attached to the specimen to ensure no damage during cut-off, was removed by wet grinding. The graphite block, now of slightly shorter length, was then reused.

---

* Metco Perkin-Elmer
Westbury, NY 11590

†Blend A-99-53. supplied courtesy of Muscle Shoals Minerals Tuscumbia, Alabama 35674

‡Grade HLM. supplied courtesy of Great Lakes Carbon Corporation Briarcliff Manor, New York 10510

Each specimen (2.5cm x 7.5cm x .09cm) was then cut into four flexural test specimens (1.25cm x 3.75cm x .09 cm) using a water-lubricated diamond cut-off saw.

Composite specimens were produced by spraying a mechanical mixture of Al_2O_3 -20 vol.% (17 wt.%) a-silicon carbide♦. Three sizes of SiC reinforcing particle were examined:

62 µm
46 µm
30 µm

Identical spray parameters (Table 1) and fabrication techniques were used for Al_2O_3 and Al_2O_3 -SiC composite specimens.

3.2 X-Ray Diffractometry

X-ray diffractometry (XRD) was carried out in order to determine the phase constituency of as-received powders, as-sprayed deposits, and heat treated deposits. Scans were run over a 2θ spectrum of 20-80º at a scan rate of 1 deg.min^{-1}. Cu Kα radiation was employed.

♦Buehler Ltd.
Silicon Carbide Powder Grit 240,
320, & 400 Lake Bluff, IL 60044

3.3 Differential Scanning Calorimetry

Differential scanning calorimetry (DSC) is a technique whereby calorimetric measurements are derived from temperature differences between the specimen and an inert standard as the system temperature is varied over the range of interest.

DSC was used to examine the conversion of metastable phases in as-sprayed deposits and to search for evidence of interfacial reactions in composite specimens. Experiments were carried out under an argon atmosphere using an Omnitherm¥ DSC 1500. The system was calibrated using a sapphire standard and alumina crucibles for the 200 – 1400 ºC temperature range.

As-sprayed Al_2O_3 and composite samples (35 mg) were heated from 200 – 1400 ºC at a ramp rate 20 ºC min -1. Inert α-alumina of comparable weight was used as a standard.

3.4 Optical Light Microscopy

Optical microscopy was used to examine deposit cross-sections and for stereographic observations of deposit surfaces. An image analysis system was used to determine the volume fraction of the reinforcing phase in composite specimens.

¥PL Thermal Sciences
Mundelein, Illinois 60060

Cross-sections were mounted in an epoxy-resin using vacuum impregnation. Specimens were ground and polished, 180 grit SiC through 1 µm diamond polish, using an automated polishing system.

3.5 Scanning Electron Microscopy

Secondary electron imaging was used to examine deposit surfaces and SiC feedstock. Back-scattered electron imaging was used to examine fracture surfaces of as-sprayed and heat treated deposits. Prior to examination, all specimens were sputter coated with gold to prevent charge buildup.

3.6 Density Measurements

Density measurements of as-sprayed and heat treated deposits were carried out using Archimedes' Principle with water as the immersion medium:

(1) $$\rho_{specimen} = \left(\frac{m}{m - m'} \right) \rho_{H_2O}$$

where

m = weight of specimen in air

m' = weight of specimen in water

ρH_2O = density of water

Reported values are the average of three measurements.

3.7 Three-Point Bend Testing

Three-point bend testing was used to determine the flexural modulus of elasticity (E_b) and ultimate flexural strength (F_b) :

$$(2) \quad E_b = \frac{L^3(\Delta P / \Delta Y)}{4bt^3}$$

And

$$(3) \quad F_b = \frac{3PL}{2bt^2} \ (N/m^2)$$

where:

P = Total applied load (newtons).
L = Test span (meters).
b = Measured width of specimen (meters).
t = Measured thickness of specimen (meters)
($\Delta P / \Delta Y$) = Slope of the initial portion of the load deflection curve which has been corrected for the testing machine spring constant[28].

In this study, the span L was set at 2.54 cm. Flexural specimens typically measured 3.75 cm x 1.25 cm x .09 cm. Each specimen was flexurally loaded at a constant crosshead speed of 5.08 x 10^{-2} cm/min until failure occurred. Load was autographically recorded as a function of crosshead movement and specimen deflection was considered equal to the crosshead displacement. A total of six flexural specimens were tested per experimental condition.

4. RESULTS AND DISCUSSION

4.1 Plasma Sprayed Al_2O_3

4.1.1 X-Ray Diffractometry and Differential Scanning Calorimetry

X-Ray Diffractometry (XRD) of the feedstock aluminum oxide showed it to consist primarily of the α (corundum) phase with trace amounts of cubic β-Al_2O_3 (Figure 3).

It is well documented that metastable γ-alumina is the prevailing phase in plasma sprayed Al_2O_3 [2,26,29]. Similar results were observed in this study. The conversion of cubic γ to the stable corundum structure occurs by a number of paths depending on the starting material and the manner in which the γ phase was prepared [30].

Differential scanning calorimetry of the as-sprayed Al_2O_3 showed two distinct reactions occurring at 860 ºC and 1220 ºC (Figure 4). These reactions were not observed during subsequent cooling and reheating cycles. For this reason, the reconversion of metastable phases is indicated.

XRD (Figure 3) showed the first exotherm, occurring at 860 ºC, to be associated with the transformation of γ -to- δ-alumina. This transformation liberated 5.6 J/g. Delta grows at the expense of gamma yet does not transform to the stable α phase until 1220 ºC. The δ-to-α transformation is accompanied

by the liberation of 41.7 J/g.

It should be noted that reported unit enthalpies for the transformation of metastable phases are likely understated: Specimens did contain some α-alumina which contributed to their mass yet did not undergo any transformations.

4.1.2 Density

Figure 5 shows the density of plasma-sprayed Al_2O_3 in the as-sprayed and heat treated conditions. Theoretical densities have been included for those conditions in which the specimen consisted entirely of α- alumina.

Significant increases in density are associated with phase transformations, namely the conversion of γ-to-δ after 4 hours at 1000 ºC and most notably the transformation of δ-to-α after 1 hour at 1300 ºC. Once phase transformations have been completed, further increases in density occurred only with significant time and temperature.

4.1.3 Mechanical Properties

Figure 6 shows the flexural modulus of elasticity and ultimate flexural strength of plasma sprayed Al_2O_3 in both the as-sprayed and heat treated conditions. A general trend of increasing modulus and strength with time and temperature was observed. Results are summarized in Table 2.

The as-sprayed modulus of 40.1 GPa (5.8 MPSI) is comparable to

reported values for plasma-sprayed ceramics[25, 26, 27]. After heat treatment of 1 hour at 1300 ºC, the plasma sprayed Al_2O_3 has undergone phase transformations and consists almost entirely of the α-alumina. A flexural modulus of 63.8 GPa (9.3 MPSI) is observed compared to 380 GPa (55 MPSI) for a sintered α-alumina of comparable density.

The degradation of properties with respect to their monolithic counterparts observed for the plasma sprayed ceramics is due, in part, to the interface between lamellae: Under most circumstances, the incorporation of high modulus, high strength fibers results in a composite material having properties superior to that of the matrix alone. In the case of a plasma-sprayed material, however, the interface between lamellae may act as low modulus, weak "fibers" which degrade the properties of sprayed deposits with respect to their monolithic counterparts. As such, the term "reciprocal composite" [31] may be used to describe the microstructure generated by plasma spraying

Decreases in modulus and strength with respect to the as-sprayed condition are observed after 4 hrs at 1000 ºC. Boch et al[26] attributed this decrease to micro-cracking due to shrinkage which accompanies the γ-to-δ transformation.

After 1 hr. at 1300 ºC, the δ-to-α transformation has occurred and flexural specimens consisted entirely of α-alumina. A significant increase in strength and modulus was observed. Although micro-cracking would be expected to accompany this transformation, since density measurements

indicate the shrinkage associated with the δ-to-α transformation is even greater than that of the γ-to-δ transformation (Figure 5), the properties of α-alumina are evidently so far improved over that of the γ and δ phases that deleterious effects which might have resulted from micro-cracking are at least partially overshadowed.

Only slight increases in modulus and strength are observed after 15 hours at 1300 ºC. No further phase transformations have occurred and the temperature appears to be too low for significant densification.

Five hours at 1500 ºC and nine hours at 1600 ºC resulted in modulii increases to 2.1 and 2.4 times that of the material heat treated for 15 hours at 1300 ºC. The magnitude of these increases exceeds that which could be expected on the basis of increased bulk density alone.

Dean and Lopez[36] used several semi-empirical equations to describe the relationship between modulus and porosity in ceramic materials:

$$(4)\quad E_p = E_o(1 - bP)$$

$$(5)\quad E_p = E_o \exp(-bP)$$

$$(6)\quad E_p = E_o \frac{(1 - P)}{(1 + bP)}$$

$$(7)\quad E_p = E_o(1 - bP + 2bP^2)$$

Where E_P is the modulus at a porosity P, E_O is the modulus of the pore-free material, and b is a coefficient dependent on the material and geometry of the

pores.

Steffens and Fisher[25] examined the elastic modulus as a function of porosity in as-sprayed $ZrO_2 - 7$ wt.% Y_2O_3. Porosity was varied by changing the spray distance and was quantified using metallographic techniques. Although a definite trend of decreasing modulus with increased porosity was observed, attempts to fit the data to any number of semi-empirical equations describing the relationship between modulus and porosity proved unsatisfactory.

It has been suggested that the presence of open porosity and the anisotropic nature of sprayed deposits made Steffens and Fisher's choice of E_O, namely that of a pore-free sintered zirconia, inappropriate and that better results might be obtained if E_O were determined by extrapolation of the experimental data.

The data of Steffens and Fisher is re-evaluated in Figure 7. Linear, polynomial, and exponential descriptions of the data are examined. The descriptions are well behaved outside the range of the data and the zero porosity modulii, E_O, obtained by extrapolation are in close agreement for all treatments of the data. . A definite, describable relationship exists between porosity and modulus in plasma sprayed ceramics.

Included in Figure 7 is the data for plasma sprayed Al_2O_3 obtained in the course of this study. Here apparent porosity was derived from density measurements and variations in density are the result of heat treatment. For each condition, samples consisted entirely of α-alumina hence phase transformations are not a consideration in the apparently erratic behavior of the

data.

Comparison with the data of Steffens and Fisher would indicate that some mechanism other than reduction in porosity, at least in the conventional sense, is responsible for the large increases in strength and modulus after the 1500 ºC and 1600 ºC heat treatments.

Boch et al [26] observed significant improvements in modulus to coincide with a reduction of interlamellar microporosity during the severe heat treatment of plasma sprayed Al_2O_3. Metallographic and flexural results of this study are consistent with these observations and suggest that with severe heat treatment, a sintering of adjacent lamellae occurs to improve the degree of interlamellar bonding, and thus, the bulk properties of the deposit.

4.1.4 SEM Fractography.

Figure 8 shows the fracture surfaces of as-sprayed and sintered Al_2O_3 deposits. Back scattered electron imaging was used at magnifications of 250 and 500. It is observed that the fracture surface of the as-sprayed condition (A,C) is quite jagged in comparison to that of the deposit heat treated at 1500 ºC for 5 hours (B,D).

Fracture in a plasma sprayed ceramics may occur by a combination of interlamellar and intralamellar mechanisms (Figure 9). In the former cracks propagate along the interface between splats while in the latter a cleavage of the individual lamellae occurs.

The tortuous fracture surface of the as-sprayed deposit suggests that crack growth has proceeded to a large extent along the poorly bonded interface between lamellae.

The more planar fracture surface of the heat treated deposit implies that an intralamellar mechanism was more prominent in its failure: After suitable heat treatment, a sintering of adjoining lamellae eliminates the conspicuous path for crack growth.

4.1.5 Load-Deflection Behavior of As-Sprayed and Sintered Deposits

Figure 10 illustrates representative load-deflection curves for as-sprayed and sintered Al_2O_3 deposits. Salient features of the as-sprayed condition include a pseudo-plastic region, large deflection prior to ultimate failure, and failure requiring sustained load. The sintered deposit is more typical of a conventional ceramic material; a linear relationship between load and deflection followed by catastrophic failure.

Berndt[24] attributed pseudoplastic behavior, observed during tensile adhesion testing of ZrO_2 - 8 wt. % Y_2O_3, to lamellae sliding past one another in a partially reversible manner.

Siemers and Meehan[27] utilized four-point bend testing in conjunction with acoustic emission (AE) to examine the properties of ZrO_2 - 24wt.% MgO. Significant AE activity, beginning at loads less than one half of that required to

produce ultimate failure, was reported. Upon cyclic loading no AE activity was observed until the previous load was reached. Pseudoplastic behavior as manifested by a non-linear load-deflection relationship was attributed to the opening of cracks, more likely than not, along the interlamellar defect region.

It is probable that the ability to relieve elastic strain energy through microcracking and delamination along the interfacial boundary is responsible for the strain tolerance of as-sprayed Al_2O_3 observed in this study.

The requirement of a sustained load for continuation of the failure process observed in this study, coupled with significant AE activity at loads well below those required to produce failure observed by Siemers and Meehan[27], suggests that crack growth rather than initiation controls the overall failure process in as-sprayed ceramic deposits. The tortuous crack path observed for as-sprayed deposits is consistent with such a mechanism.

The catastrophic brittle fracture observed in sintered deposits indicates that the converse is true, namely that crack initiation rather than growth controls failure after suitable heat-treatment.

4.2 PLASMA SPRAYED Al_2O_3 -SiC COMPOSITES

4.2.1 Composite Microstructures

Ceramic matrix composites were fabricated by plasma spraying a mechanical mixture of Al_2O_3 - 20 vol.% particulate SiC. Three sizes of reinforcing particle were examined: 30 µm, 46 µm, and 62 µm (Figure 11 A). It was observed that plasma spraying produced a uniform distribution of the reinforcing phase (Figure 11 B).

A preliminary study was carried out to determine the effect of plasma flame interaction on particulate SiC. A 46 µm particle size a SiC was fed into a 35 kw plasma jet, sprayed into water and examined using SEM (Figure 12). Although a slight scorching of the surface was observed, the particles did not appear to significantly degrade during the spray process.

When sprayed as a mixture with 80 vol.% aluminum oxide, a phenomenon not noted in the preliminary study was observed: At some point during their interaction with the plasma flame a significant fraction of the SiC particles "melted" or partially "melted" as indicated by their splatting behavior and lamellar structure when viewed in cross-section (Figure 13). Although incongruent melting of SiC under extreme conditions has been reported [32,33], it is generally accepted that SiC undergoes pyrolysis other than melting. No SiC peaks were observed in XRD patterns obtained from composite specimens. Although silica formation is likely in the oxygen-containing plasma, the exact nature of the

re-solidified material observed in this study remains uncertain.

It was generally observed that the composites consisted of both particulate SiC and re-solidified inclusions (Figure 14). Quantitative metallography of composite cross-sections was performed to determine the volume fraction of the reinforcing phase. It should be noted in the following results that reinforcement refers to the sum of particulate SiC and re-solidified inclusions:

30 µm SiC: Al_2O_3 - 3.5 vol.% reinforcement (Figure 15)

46 µm SiC: Al_2O_3 - 4.2 vol.% reinforcement (Figure 16)

62 µm SiC: Al_2O_3 - 4.9 Vol.% reinforcement (Figure 17)

As all composites were fabricated by plasma spraying a mechanical mixture of Al_2O_3- 20 vol.% SiC, considerable loss of SiC occurred during the spray process.

The incorporation of an unmelted particle in a plasma sprayed ceramic is a probabilistic event: The correct interaction with molten or partially molten material is required so that the unmelted particle is in some way bonded to the deposit. For this reason, much of the particulate SiC would simply bounce off and be blown away during the spray process. Agglomeration of SiC with the Al_2O_3 could provide a more effective means of delivering the second phase so that it is incorporated into the deposit.

Degradation of SiC during interaction with the plasma effluent may also contribute to decreased loading. The experimentally observed result of

decreased reinforcement loading with decreasing SiC particle size is consistent with such a result since smaller particles would more readily vaporize or otherwise react.

4.2.2 X-Ray Diffractometry and Differential Scanning Calorimetry

X-Ray diffraction patterns obtained from both as-sprayed and heat treated composites were identical to those obtained from the unreinforced material. No SiC peaks were observed in the the as-sprayed or heat treated conditions.

Differential scanning calorimetry of composite specimens showed no evidence of interfacial reactions and the reconversion of metastable phases was identical to that observed in unreinforced deposits (Figure 4).

4.2.3 Composite Density

The similarity in density between SiC and Al_2O_3 coupled with small reinforcement loading placed any differences in density between Al_2O_3 and Al_2O_3 - SiC composite specimens beyond the resolution of the technique. The experimentally obtained densities for composite specimens in both the as-sprayed and heat treated conditions are summarized in Tables 3, 4, and 5.

4.2.4 Mechanical Properties

No differences in load-deflection behavior between composite and unreinforced specimens were observed.

Figure 18 illustrates the flexural modulus of elasticity for composite specimens in both the as-sprayed and heat treated conditions. The properties of the unreinforced matrix material have been included for comparison. With the exception of the as-sprayed condition, it was observed that the incorporation of a reinforcing phase enhanced the modulus of the plasma sprayed ceramic. A similar trend was observed for the ultimate flexural strength (Figure 19).

Referring to Figures 18 and 19, it was observed that in the as-sprayed condition, composites exhibited mechanical properties inferior to those of the pure matrix material. In the case of poor bonding between the matrix and reinforcing phase, the reinforcing phase would effectively behave as porosity.

It has been shown in Figure 8 that the porosity dependence of elastic modulus in as-sprayed ceramics is adequately described by the following equations:

$$(8) \qquad Ep = E_0 \exp\{-13.79P)$$

$$(9) \qquad Ep = E_0 (1 - 9.46P + 18.728P^2)$$

$$(10) \qquad Ep = E_0 (1 - 7.926P)$$

Where Ep is the modulus at a porosity P and E_0 is the modulus of the pore free material.

Figure 20 compares the experimentally obtained modulii for as-sprayed Al_2O_3 and the composite material containing 4.9 vol.% reinforcing phase with modulii predicted by equations 8, 9, and 10. The modulus of the unreinforced Al_2O_3 deposit was used for E_0. and the volume fraction of porosity P, was set equal to 0.049, the volume fraction of the reinforcing phase. The use of 40.06 GPa, the modulus of as-sprayed Al_2O_3, as the zero porosity modulus (E_0) is appropriate since any increase in effective porosity as a result of second phase incorporation would be relative to this material.

Sound agreement between the experimentally obtained composite modulus and those predicted on the basis of the reinforcing phase behaving as porosity, supports the hypothesis of poor bonding between the matrix and reinforcing phases.

Although shrinkage associated with the γ-to-δ transformation resulted in a degradation of properties for plasma sprayed Al_2O_3, composite properties improve noticeably after 4 hrs. at 1000 ºC. It is possible that the shrinkage of the matrix has improved bonding between the matrix and reinforcing phase and allowed load transfer to occur.

The strength and modulus of composites heat treated at 1300 ºC are significantly better than those of the pure matrix material which has undergone an identical heat treatment. A high degree of load transfer is occurring between the matrix and reinforcing phases. Once again it is postulated that shrinkage of the matrix, in this case associated with the δ -to- α transformation, places the reinforcing phase in compression and the surrounding matrix in tension to create integral bonding between the matrix and reinforcing phases.

5. CONCLUSIONS

The microstructure and properties of substrate free plasma sprayed Al_2O_3 and Al_2O_3- SiC composites have been investigated.

In the as-sprayed condition plasma sprayed Al_2O_3 consists primarily of the metastable γ phase, a result of rapid solidification. The reconversion of γ – to- α occurs by two distinct reactions: the transformation of γ to δ at 860 ºC followed by the conversion of δ -to- α at 1220 ºC.

Modulus and strength values of 40.1 GPa and 50 MPa, respectively were observed for as-sprayed Al_2O_3. It is probable that the interface between lamellae act as low modulus, weak "fibers" which degrade the properties of sprayed deposits with respect to their monolithic counterparts. As such, it may be appropriate to describe the microstructure produced by plasma spraying as a "reciprocal composite".

As-sprayed Al_2O_3 exhibits pseudoplastic behavior and strain tolerance. It appears that crack growth along the interface between lamellae, as opposed to crack initiation, controls the overall failure process.

Substantial improvements in the strength and modulus of plasma sprayed Al_2O_3 have been achieved by heat treatment. These occur first as a result of the transformation of δ -to- α alumina. Then, with significant time at temperature, a sintering of adjacent lamellae occurs. This improves the degree of interlamellar bonding, and thus, the bulk properties of the deposit. Crack initiation controls the failure processes after sintering.

The degradation in properties with respect to the pure matrix material observed for the as-sprayed condition is believed to be the result of poor bonding between the matrix and reinforcing phases. With heat treatment, the reconversion of metastable phases is accompanied by significant shrinkage of the Al_2O_3 matrix. It is believed that this improves the degree of bonding between the matrix and reinforcing phases and allows the transfer of load between the matrix and reinforcing phase to occur.

Figure 1 Schematic cross-section of an in-atmosphere plasma spray gun (APS).

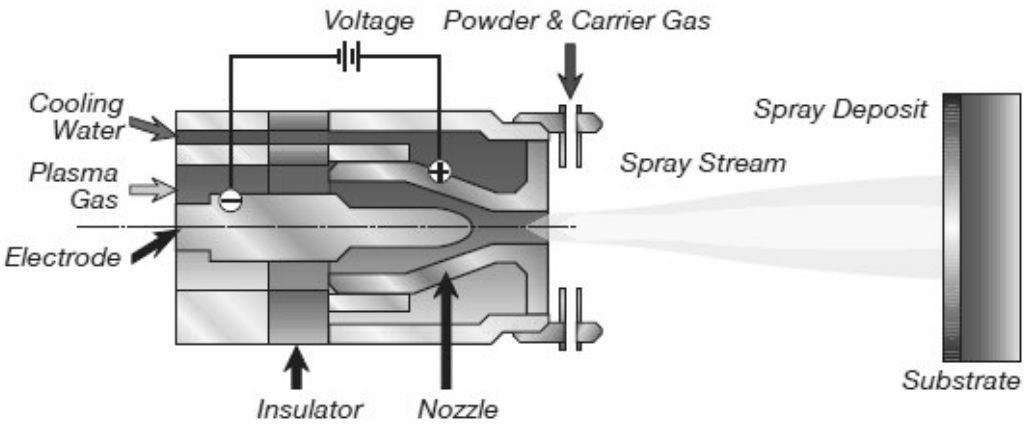
Voltage
Powder & Carrier Gas
Cooling Water
Plasma Gas
Electrode
Spray Deposit
Spray Stream
Substrate
Insulator
Nozzle

Figure 2 SEM micrographs showing the surface morphology of a plasma-sprayed Al_2O_3 deposit.
A) 200 x
B) 400 x

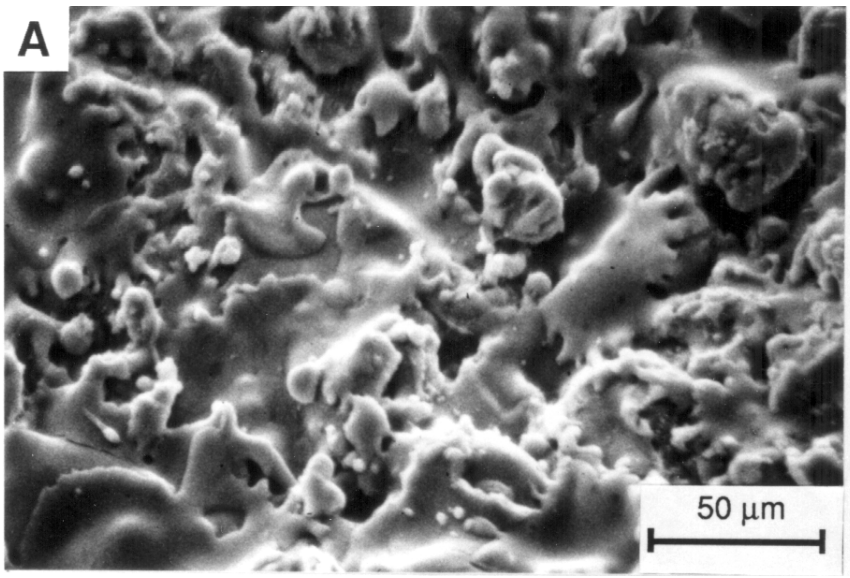
A
50 µm

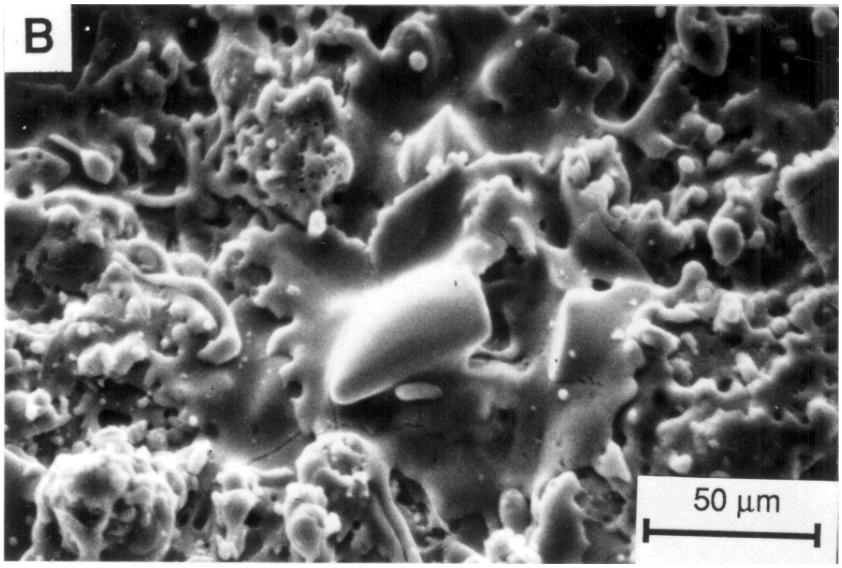
B
50 µm

Figure 3 X-ray diffraction patterns from as-received Al_2O_3 feedstock, plasma-sprayed Al_2O_3 in the as-sprayed condition, heat treated at 1000 ºC for 4 hours, and after 1 hour at 1300 ºC

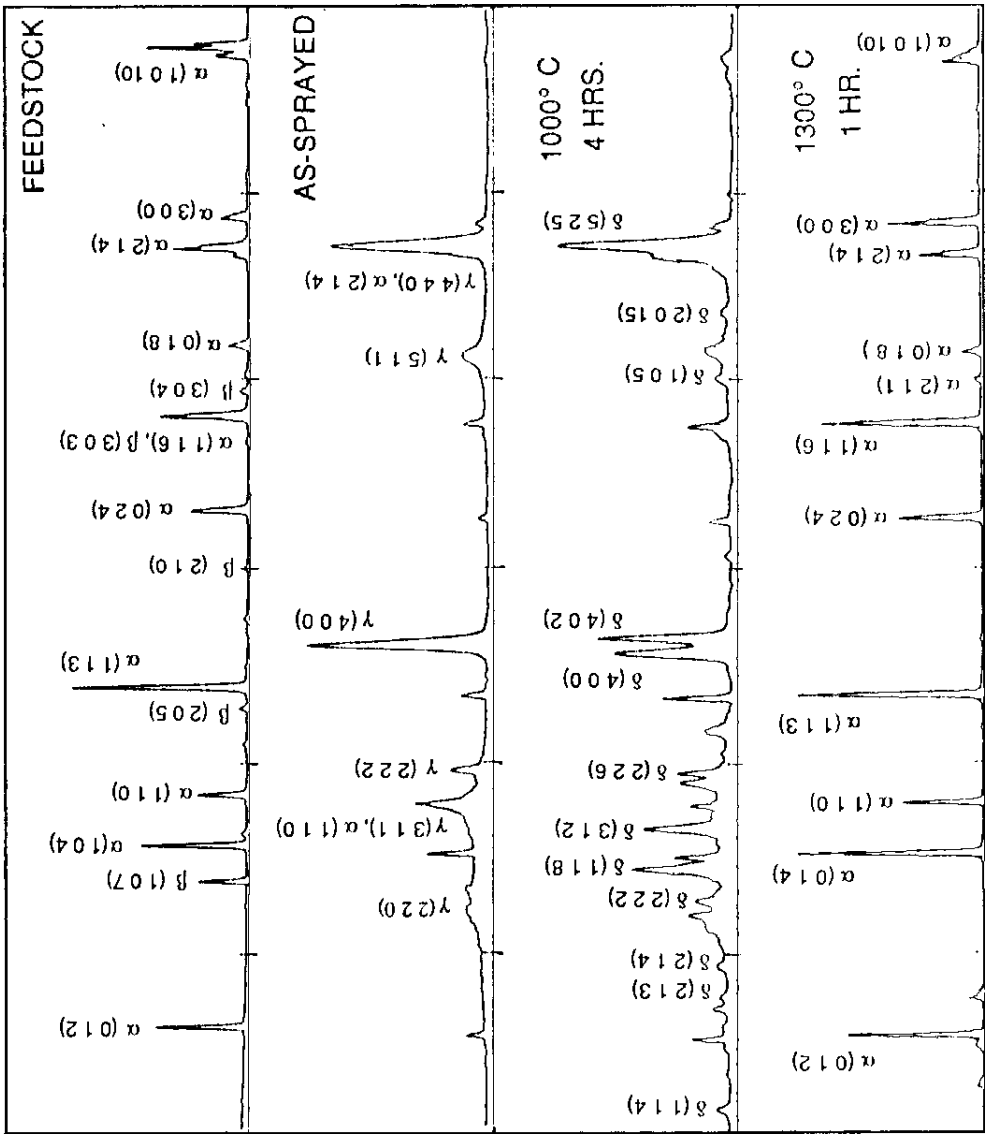
FEEDSTOCK
α (0 1 2)
β (1 0 7)
α(1 0 4)
α (1 1 0)
β (2 0 5)
α (1 1 3)
β (2 1 0)
α (0 2 4)
α (1 1 6), β (3 0 3)
β (3 0 4)
α (0 1 8)
α (2 1 4)
α (3 0 0)
α (1 0 10)
AS-SPRAYED
γ(2 2 0)
γ(3 1 1), α (1 1 0)
γ (2 2 2)
γ (4 0 0)
γ (5 1 1)
γ (4 4 0), α (2 1 4)
1000° C
4 HRS.
δ (1 1 4)
δ (2 1 3)
δ (2 1 4)
δ (2 2 4)
δ (1 1 8)
δ (3 1 2)
δ (2 2 6)
δ (4 0 0)
δ (4 0 2)
δ (1 0 5)
δ (2 0 15)
δ (5 2 5)
1300° C
1 HR.
α (0 1 2)
α (0 1 4)
α (1 1 0)
α (1 1 3)
α (0 2 4)
α (1 1 6)
α (2 1 1)
α (0 1 8)
α (2 1 4)
α (3 0 0)
α (1 0 10)

Figure 4 DSC thermogram obtained during the heating of plasma-sprayed Al_2O_3. The exothermic transformation of γ-to-δ at 860 ºC is followed by the conversion of δ-to-α at 1220 ºC

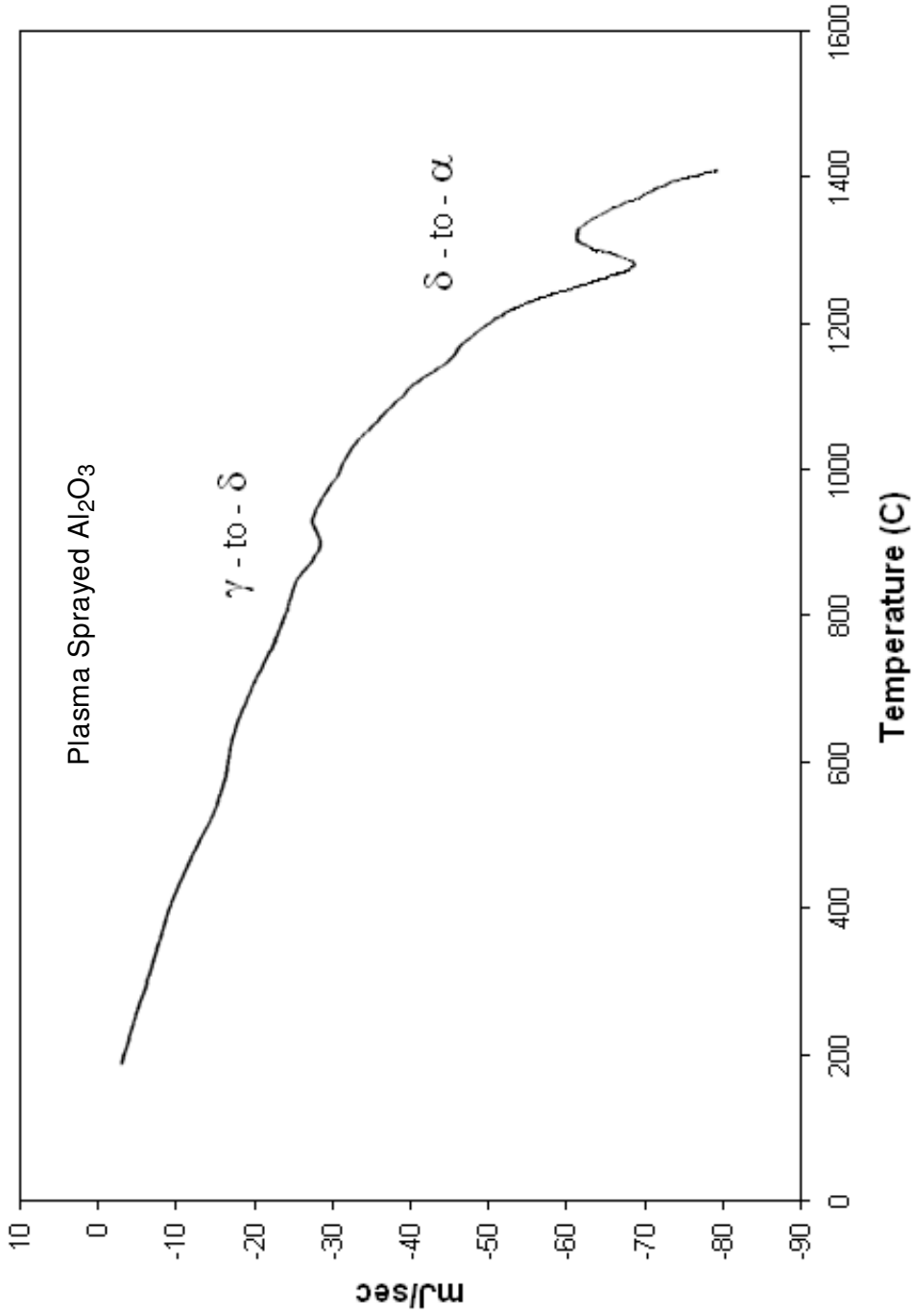
Plasma Sprayed Al_2O_3
γ - to - δ
δ - to - α
mJ/sec
Temperature (C)
10
0
-10
-20
-30
-40
-50
-60
-70
-80
-90
0
200
400
600
800
1000
1200
1400
1600

Figure 5 The density of plasma sprayed Al_2O_3 in as-sprayed and heat treated conditions. Theoretical densities have been included for those conditions in which the specimen consisted entirely of α -alumina

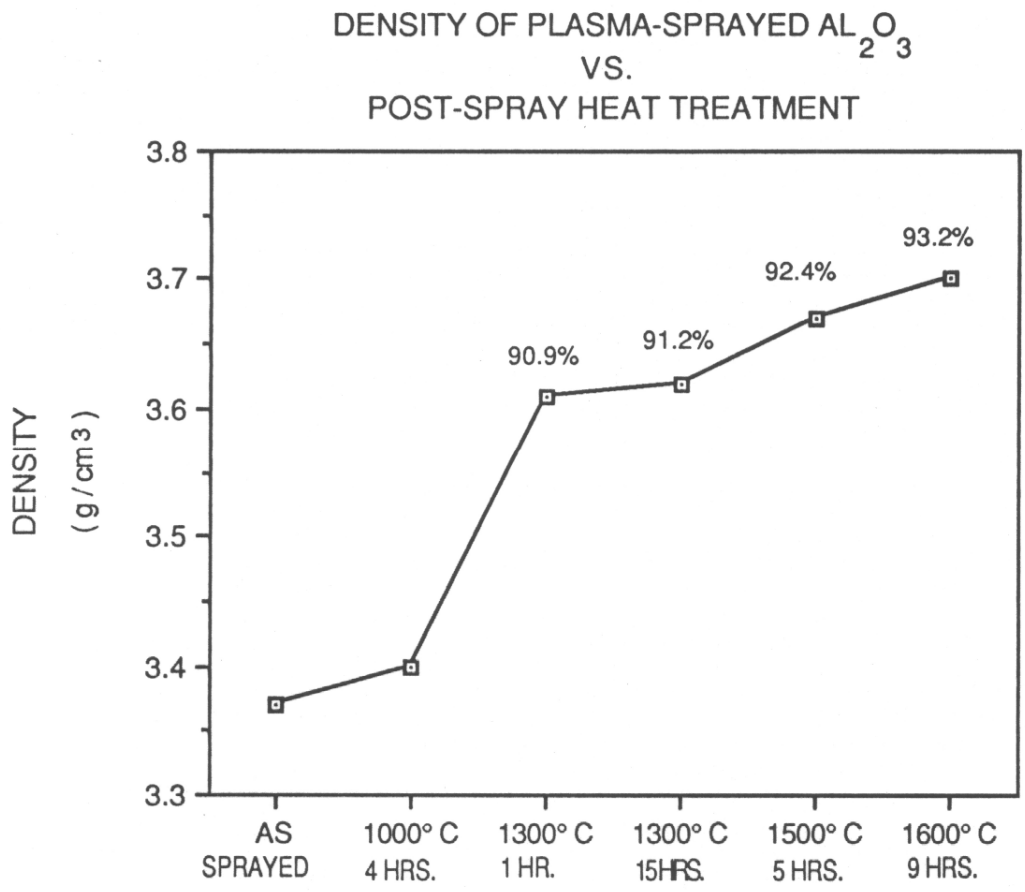
DENSITY OF PLASMA-SPRAYED AL2O3
VS.
POST-SPRAY HEAT TREATMENT
DENSITY
(g / cm 3)
3.8
3.7
3.6
3.5
3.4
3.3
90.9%
91.2%
92.4%
93.2%
AS SPRAYED
1000° C 4 HRS.
1300° C 1 HR.
1300° C 15HRS.
1500° C 5 HRS.
1600° C 9 HRS.

Figure 6 The flexural modulus of elasticity and ultimate flexural strength of plasma-sprayed Al_2O_3 in as-sprayed and heat treated conditions

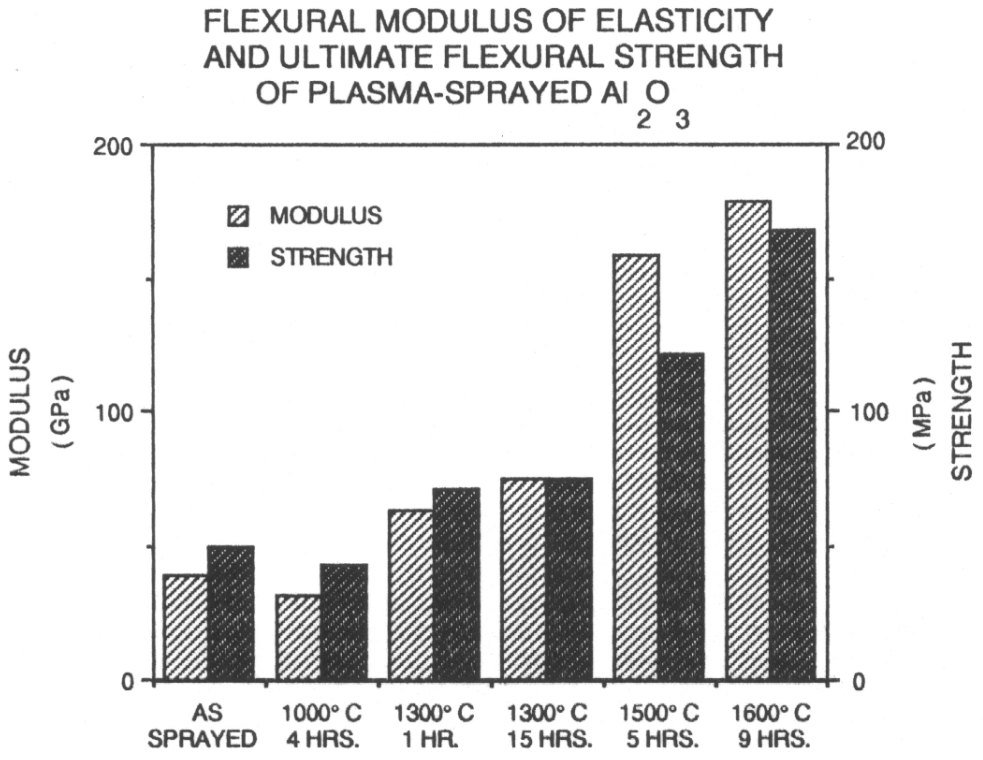
FLEXURAL MODULUS OF ELASTICITY
AND ULTIMATE FLEXURAL STRENGTH
OF PLASMA-SPRAYED Al2O3
MODULUS
STRENGTH
MODULUS (GPa)
STRENGTH (MPa)
200
100
0
AS SPRAYED
1000° C 4 HRS.
1300° C 1 HR.
1300° C 15 HRS.
1500° C 5 HRS.
1600° C 9 HRS.

Figure 7 Modulus of elasticity as a function of porosity in plasma-sprayed ceramics. Steffens and Fischer[25] varied the porosity of ZrO_2 by changing the spray distance. Variations in the density of Al_2O_3 are the result of heat treatment.

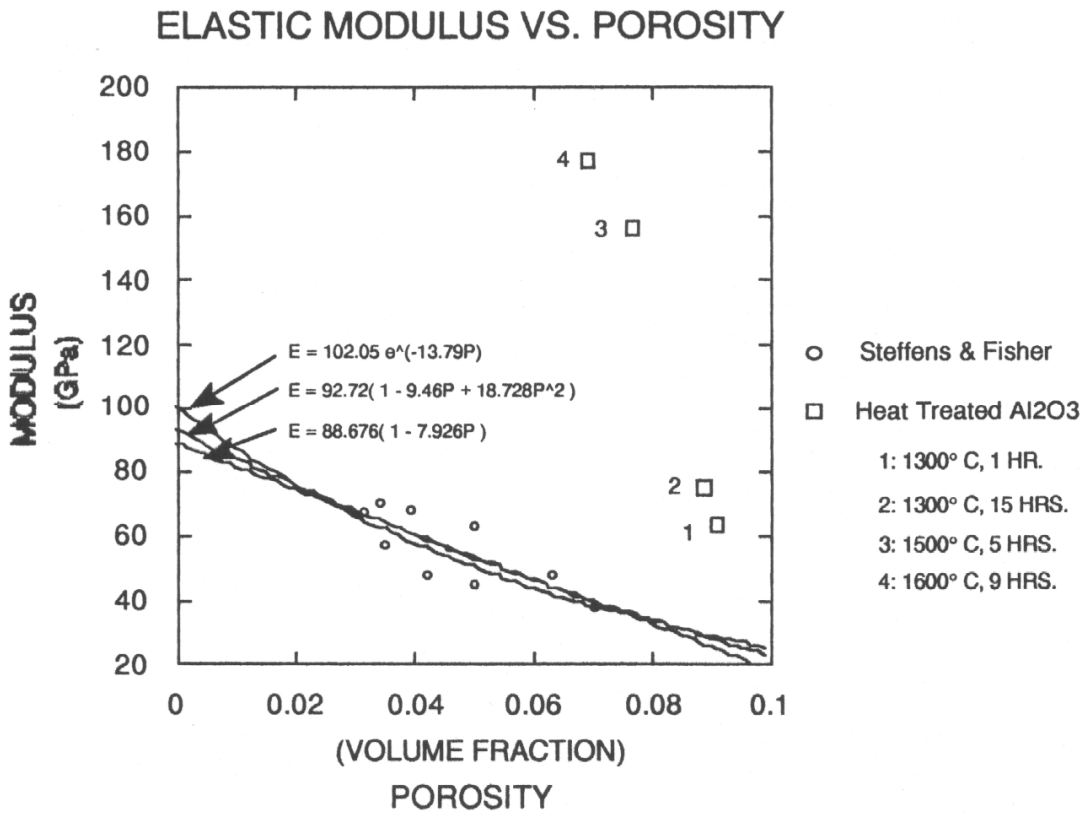
ELASTIC MODULUS VS. POROSITY
MODULUS (GPa)
200
180
160
140
120
100
80
60
40
20
0
0.02
0.04
0.06
0.08
0.1
(VOLUME FRACTION) POROSITY
E = 102.05 e^(-13.79P)
E = 92.72(1 - 9.46P + 18.728P^2)
E = 88.676(1 - 7.926P)
4
3
2
1
Steffens & Fisher
Heat Treated Al2O3
1: 1300° C, 1 HR.
2: 1300° C, 15 HRS.
3: 1500° C, 5 HRS.
4: 1600° C, 9 HRS.

Figure 8 Backscattered SEM micrographs of fracture surfaces in plasma-sprayed Al_2O_3 deposits.

As-sprayed:

A) 250 x
B) 500 x

Heat treated at 1500 ºC for 5 hours:

C) 250 x
D) 500 x

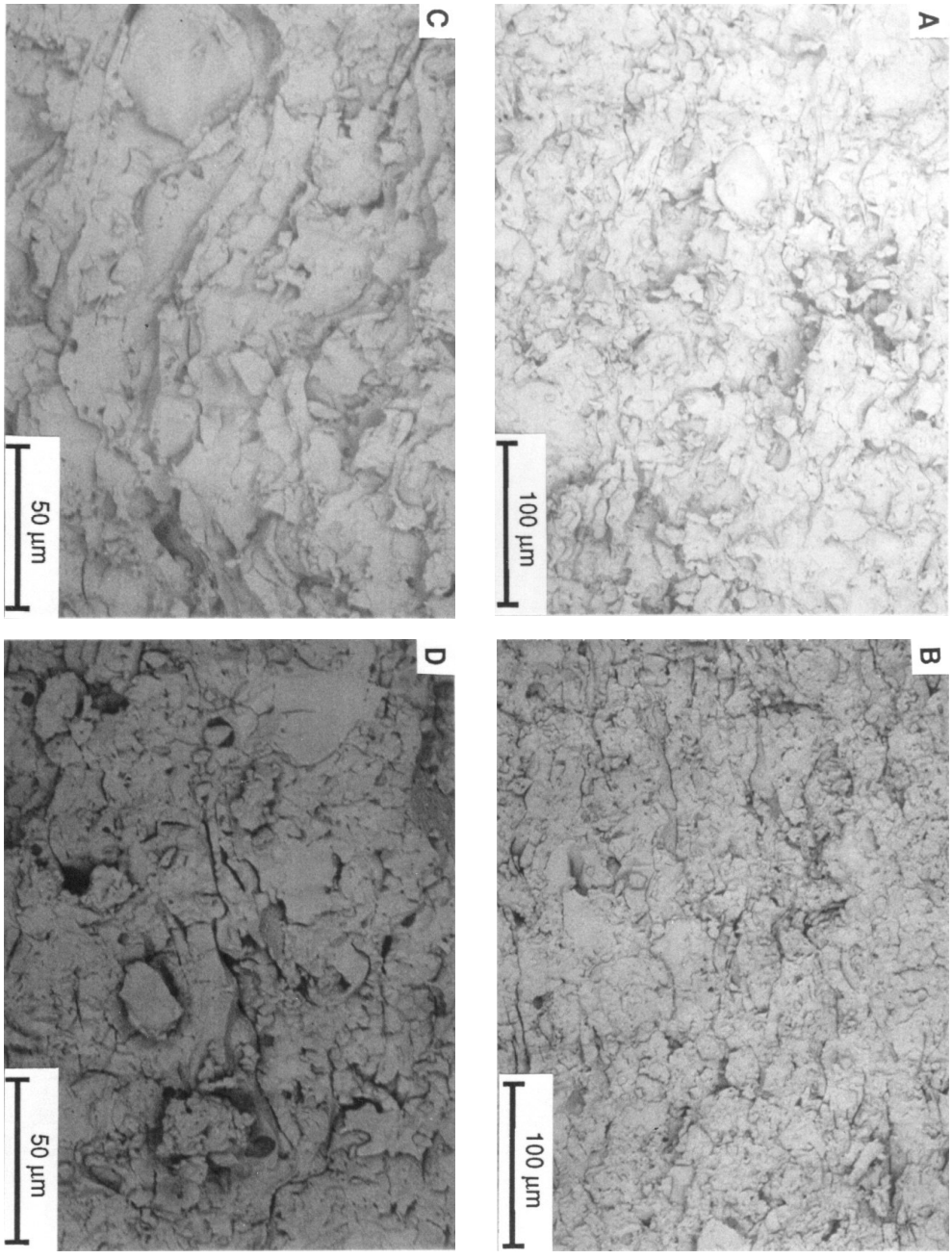
A
100 µm
B
100 µm
C
50 µm
D
50 µm

Figure 9 Schematic of inter-lamellar and intra-lamellar fracture mechanisms. In the former cracks propagate primarily along the interface between lamellae while in the latter, the cleavage of individual lamellae occurs to a greater extent.

Inter-lamellar Fracture of a Plasma-Sprayed Ceramic

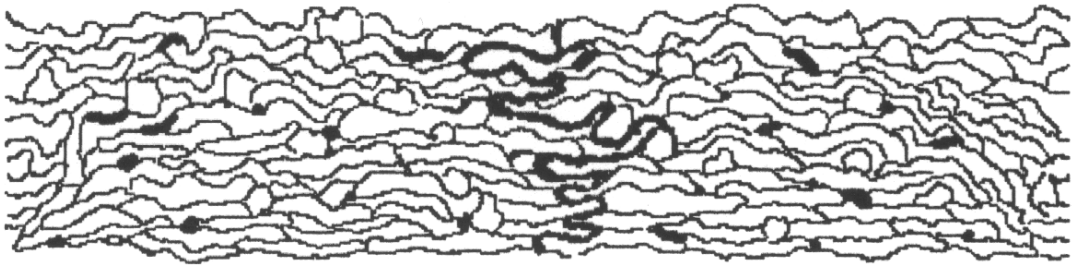

Intra-lamellar Fracture of a Plasma-Sprayed Ceramic

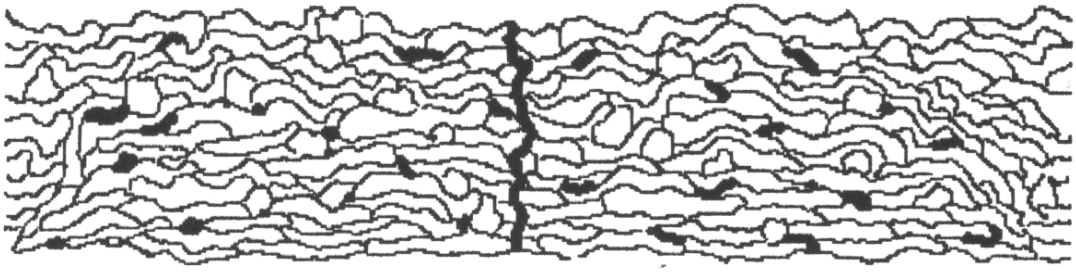

Figure 10 Representative Load-Deflection curve obtained during the three-point flexural testing of as-sprayed and heat treated deposits.

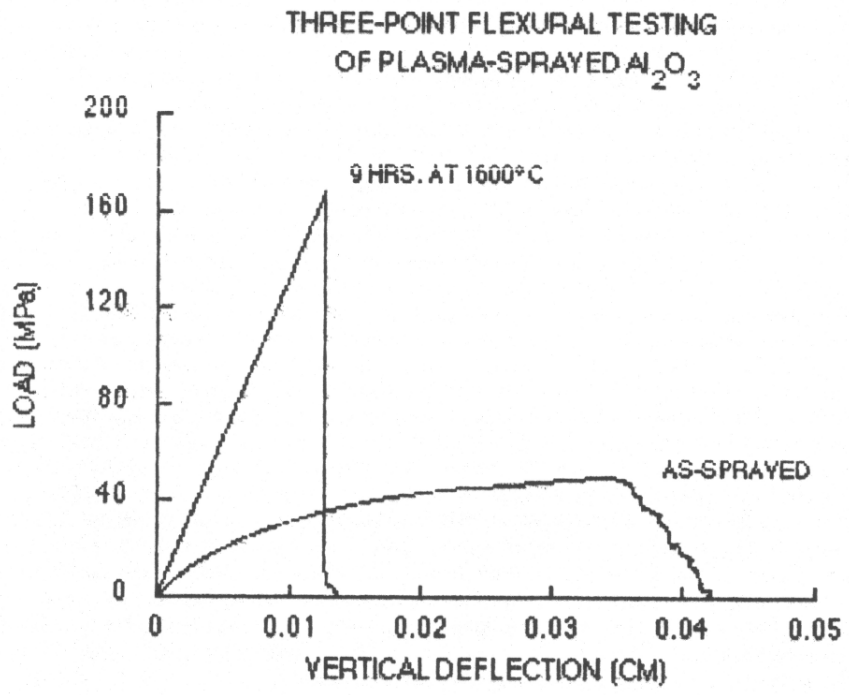
THREE-POINT FLEXURAL TESTING
OF PLASMA-SPRAYED Al_2O_3
LOAD (MPa)
200
160
120
80
40
0
9 HRS. AT 1600°C
AS-SPRAYED
0
0.01
0.02
0.03
0.04
0.05
VERTICAL DEFLECTION (CM)

Figure 11

A) Plasma-sprayed Al_2O_3 and Al_2O_3-SiC composite flexural specimens. From left to right the specimens consist of pure Al_2O_3 and Al_2O_3 reinforced with 62 µm SiC, 46 µm SiC, and 30 µm SiC respectively.

B) Optical stereo-micrograph of the surface of an Al_2O_3 - 4.9 Vol.% SiC composite specimen. The pictured specimen was fabricated using 62 µm SiC. A uniform distribution of the reinforcing phase was achieved by plasma spraying (50 x).

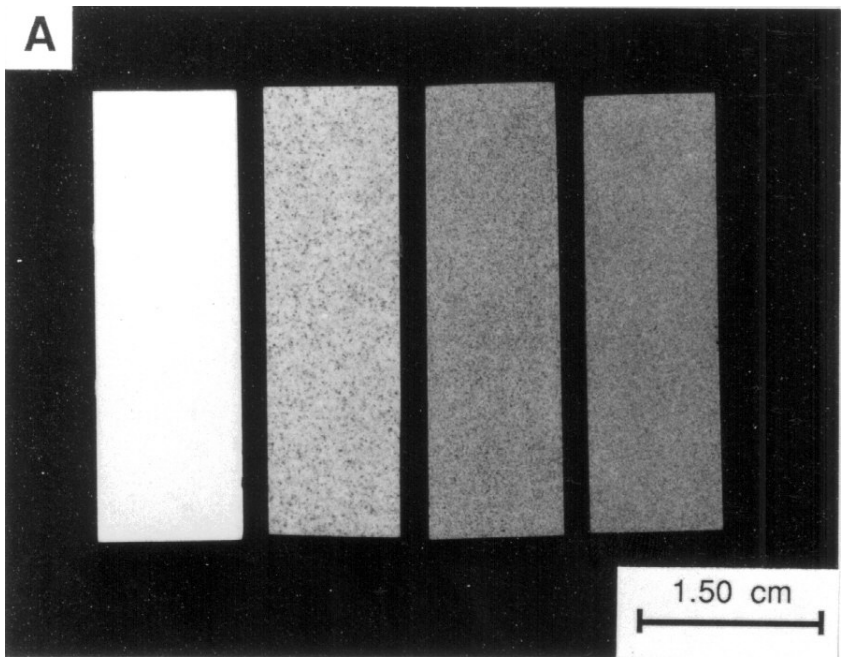
A
1.50 cm

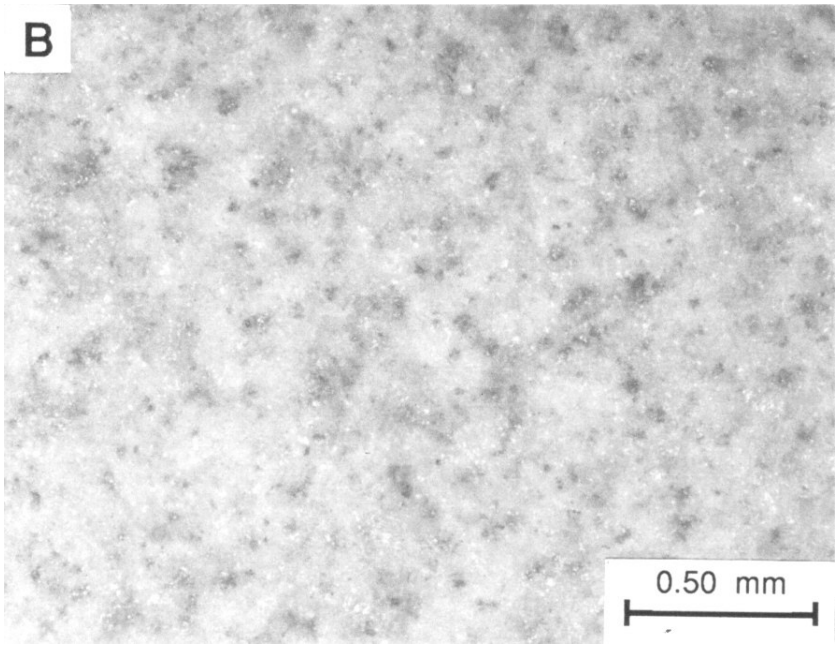
B
0.50 mm

Figure 12 SEM micrographs of particulate a-SiC (400 x).
A) As-received.
B) Pasma-Sprayed and collected in water.

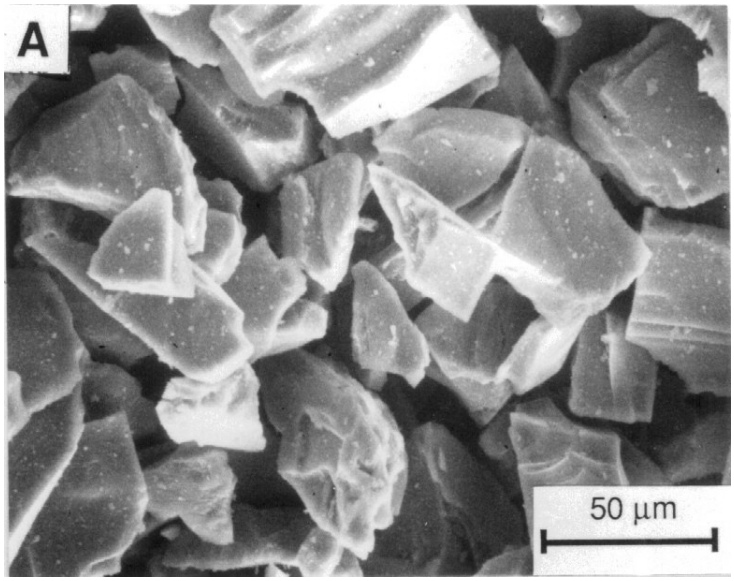
A
50 µm

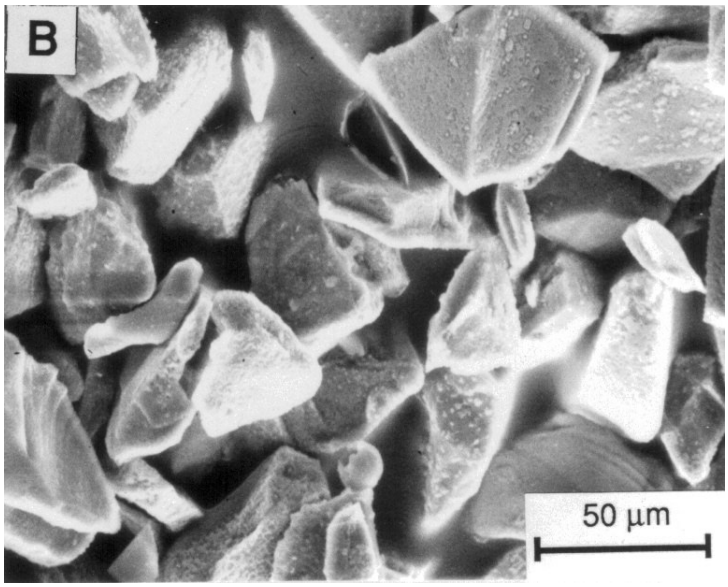
B
50 µm

Figure 13 A) Optical stereomicrograph of a re-solidified SiC splat on the surface of a plasma-sprayed composite (160 x).

B) Optical cross-section of a re-solidified inclusion in an Al_2O_3 matrix (500 x).

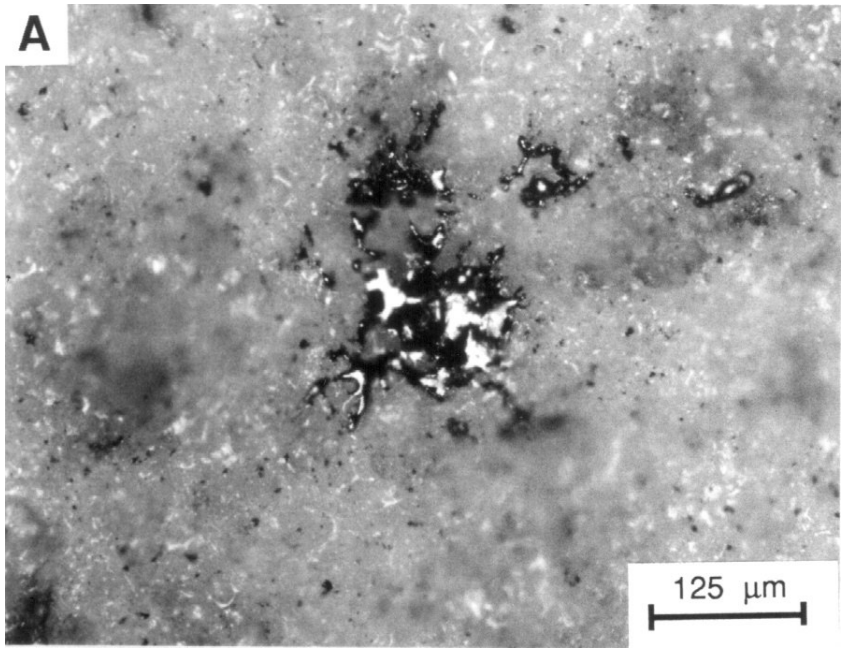
A
125 µm

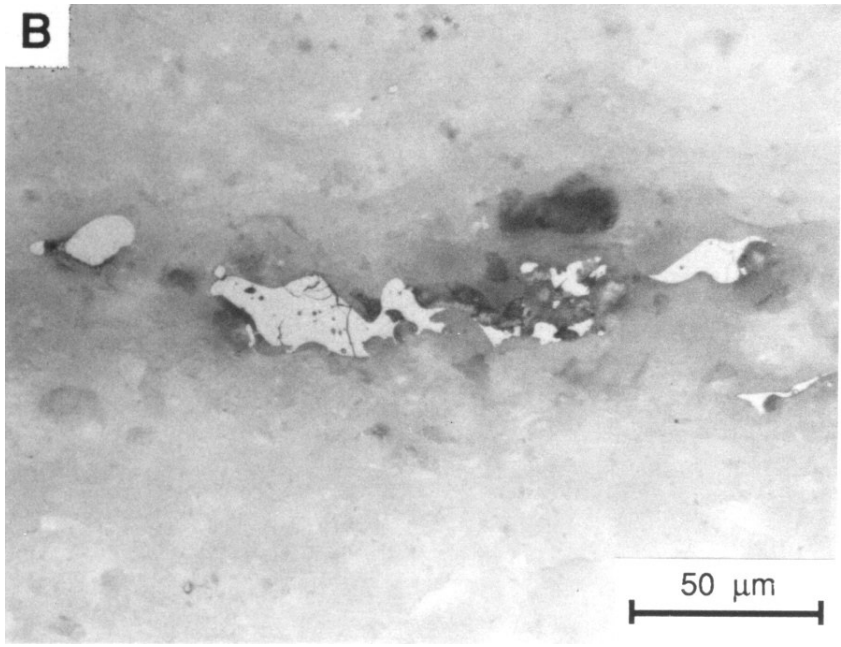
B
50 µm

Figure 14 Optical cross-section of an Al_2O_3-SiC composite showing the presence of un-melted SiC particulate, indicated by a sharp angular appearance, and re-solidified inclusions, characterized by a lamellar structure (900x)

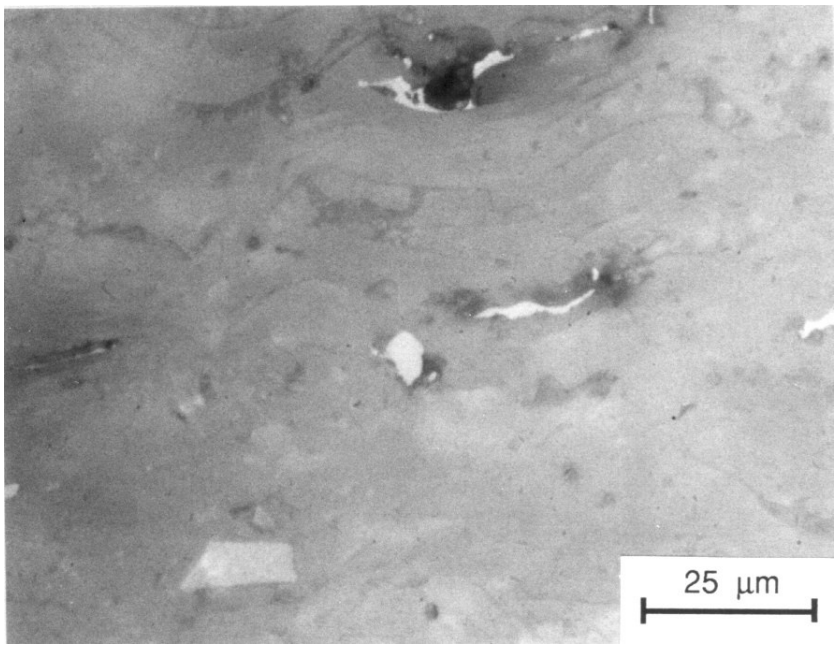
25 µm

Figure 15 Optical cross-section of a plasma-sprayed composite. Al_2O_3-3.5 vol. % reinforcement (30 µm SiC).
A) 100 x
B) 200 x

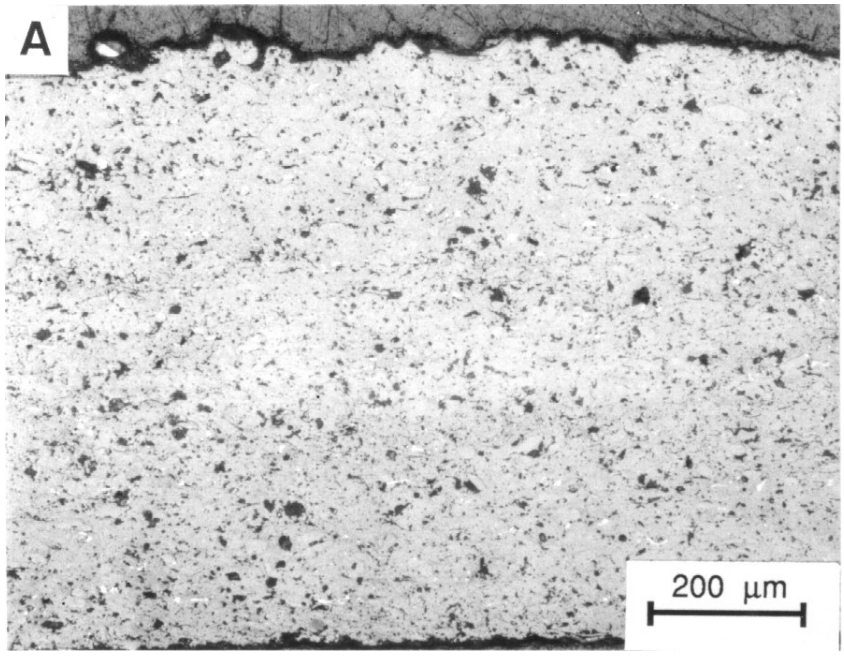
A
200 µm

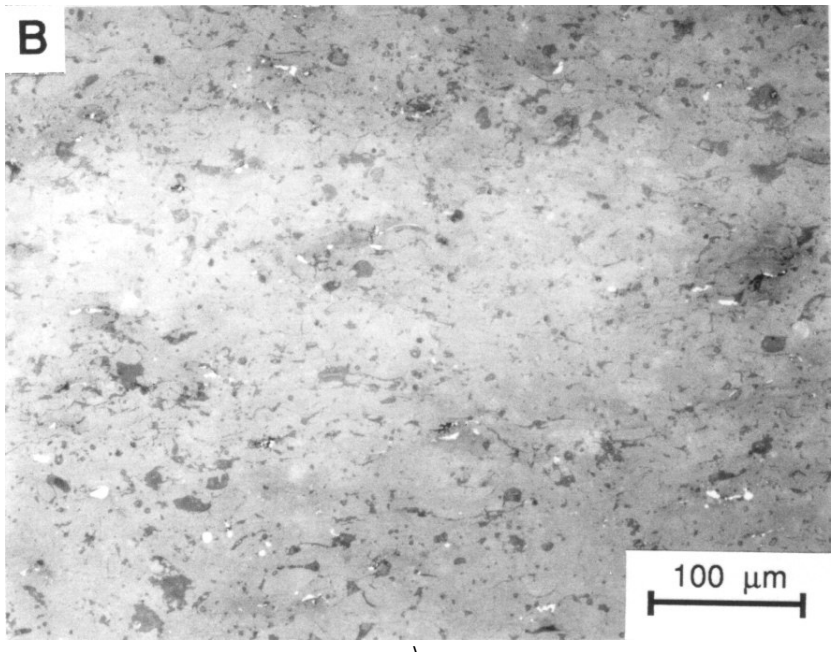
B
100 µm

Figure 16 Optical cross-section of a plasma-sprayed composite. Al_2O_3-4.2 vol. % reinforcement (46 µm SiC).
A) 100 x
B) 200 x

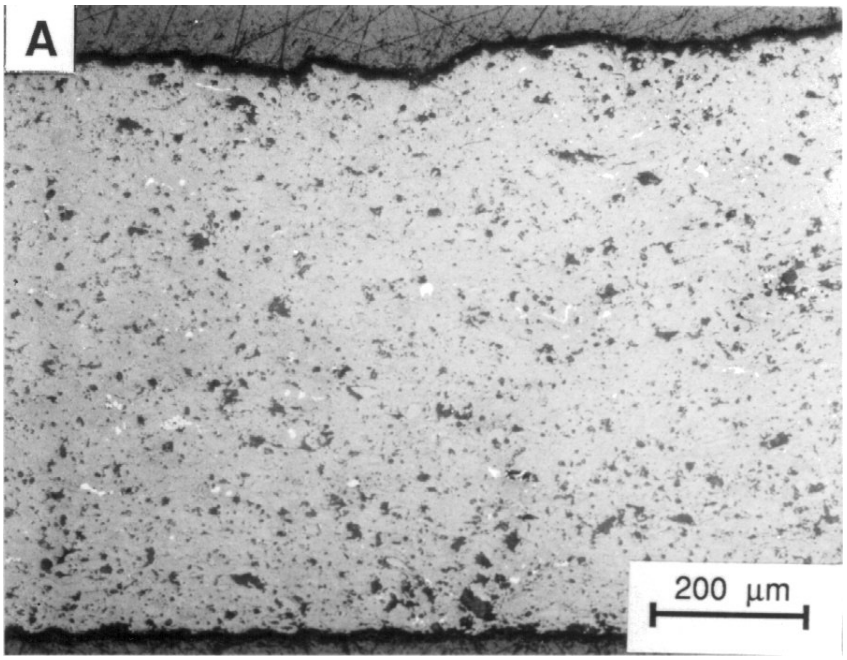
A
200 µm

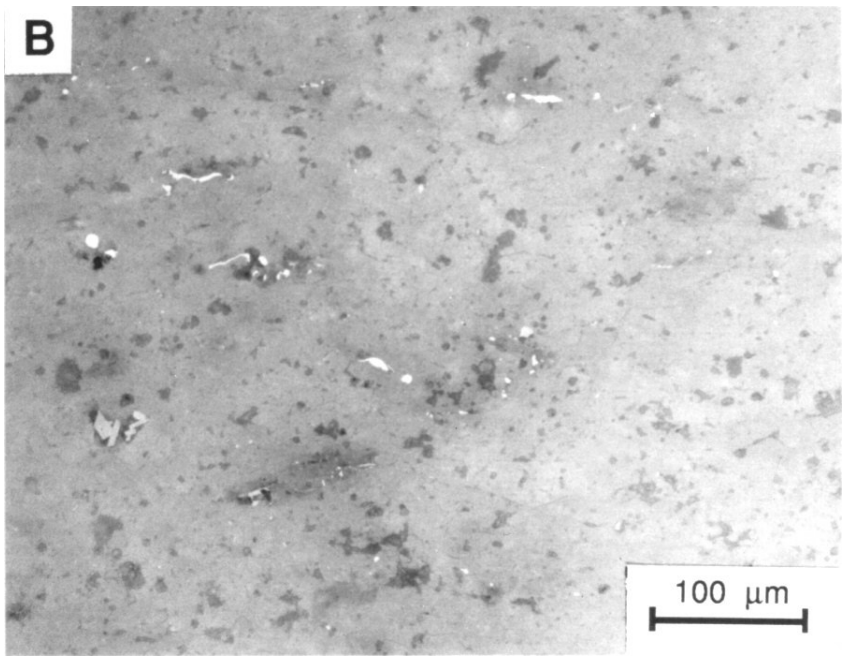
B
100 µm

Figure 17 Optical cross-section of a plasma-sprayed composite. Al_2O_3-4.9 vol.% reinforcement (62 µm SiC).
A) 100 x
B) 200 x

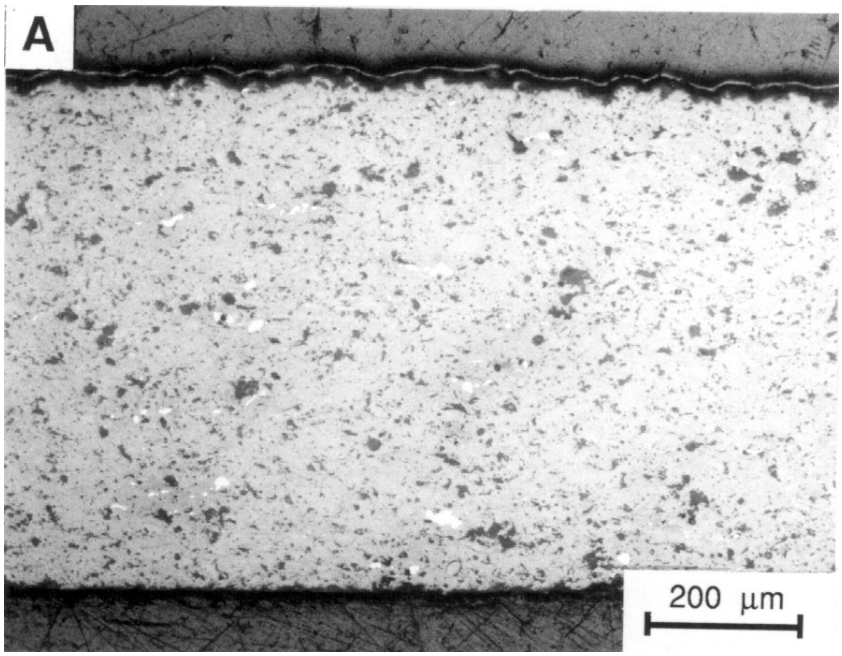
A
200 µm

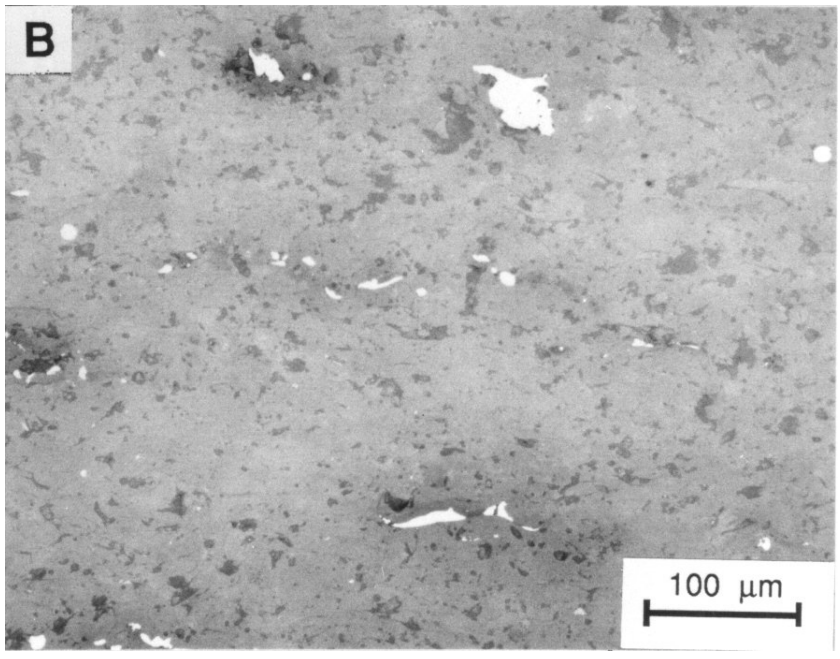
B
100 µm

Figure 18 Flexural modulus of elasticity of plasma-sprayed Al_2O_3-SiC composites in the as-sprayed and heat treated conditions.

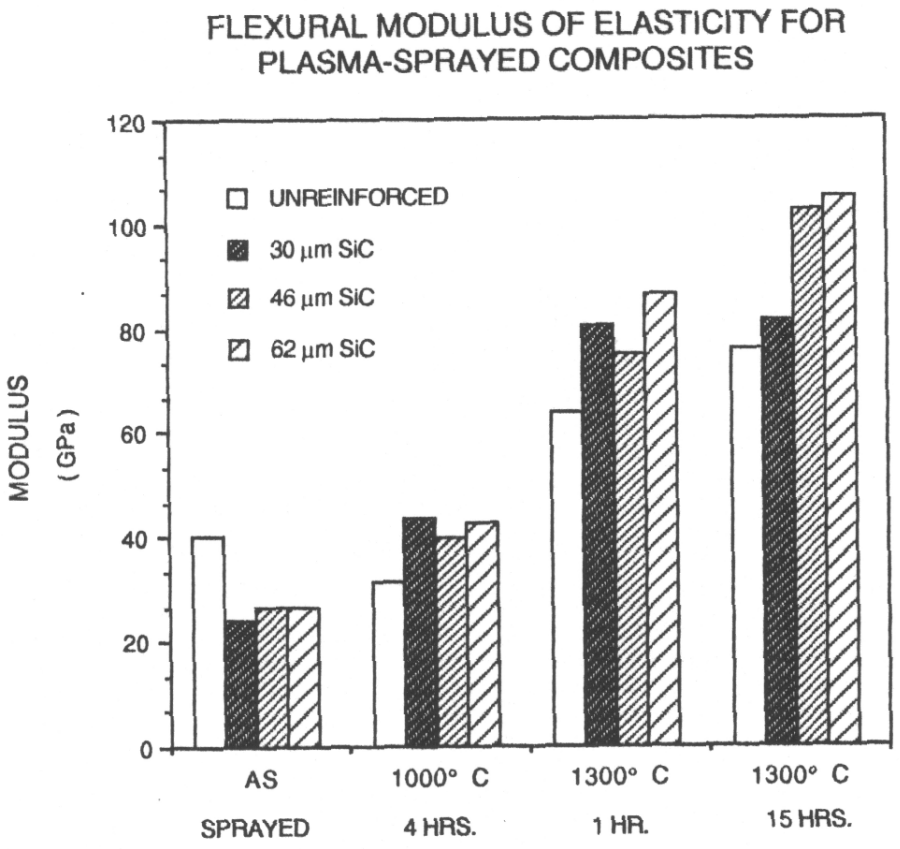
FLEXURAL MODULUS OF ELASTICITY FOR
PLASMA-SPRAYED COMPOSITES
MODULUS
(GPa)
120
100
80
60
40
20
0
UNREINFORCED
30 μm SiC
46 μm SiC
62 μm SiC
AS
SPRAYED
1000° C
4 HRS.
1300° C
1 HR.
1300° C
15 HRS.

Figure 19 Ultimate flexural strength of plasma-sprayed Al_2O_3-SiC composites in the as-sprayed and heat treated conditions.

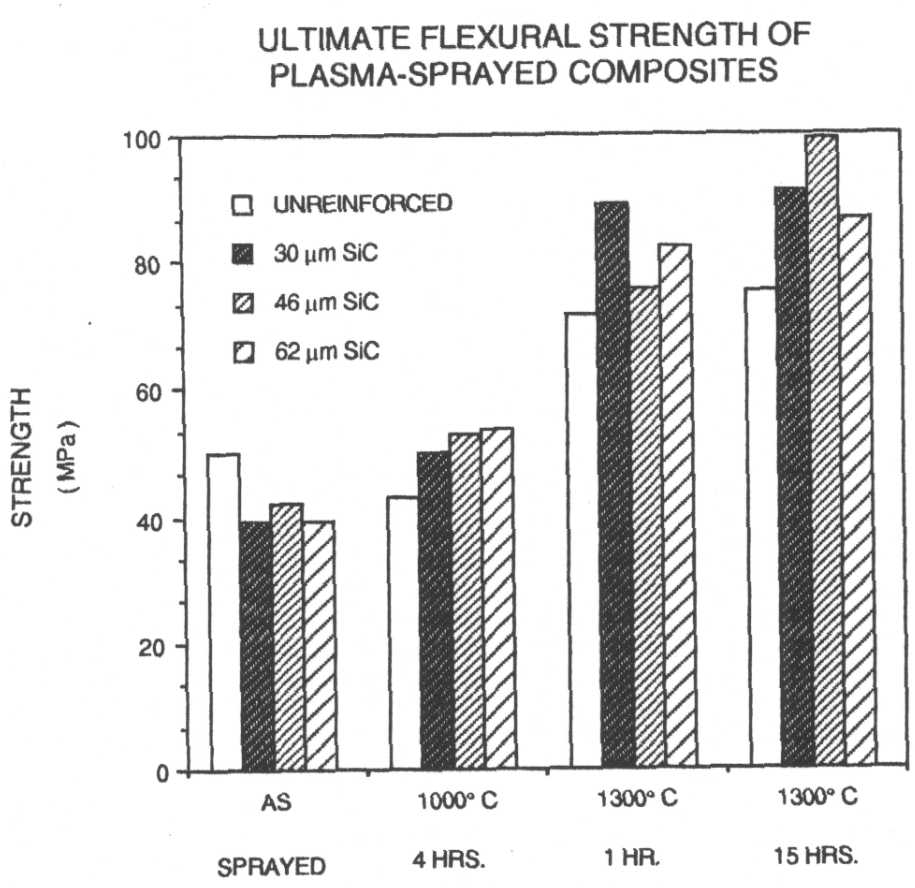
ULTIMATE FLEXURAL STRENGTH OF
PLASMA-SPRAYED COMPOSITES
STRENGTH
(MPa)
100
80
60
40
20
0
UNREINFORCED
30 μm SiC
46 μm SiC
62 μm SiC
AS
SPRAYED
1000° C
4 HRS.
1300° C
1 HR.
1300° C
15 HRS.

Figure 20 Comparison of an experimentally determined composite modulus with modulii predicted by assuming that poor bonding between the matrix and reinforcing phase would cause the reinforcing phase to behave as porosity. The modulus of unreinforced Al_2O_3 in the as-sprayed condition has been included for comparison.

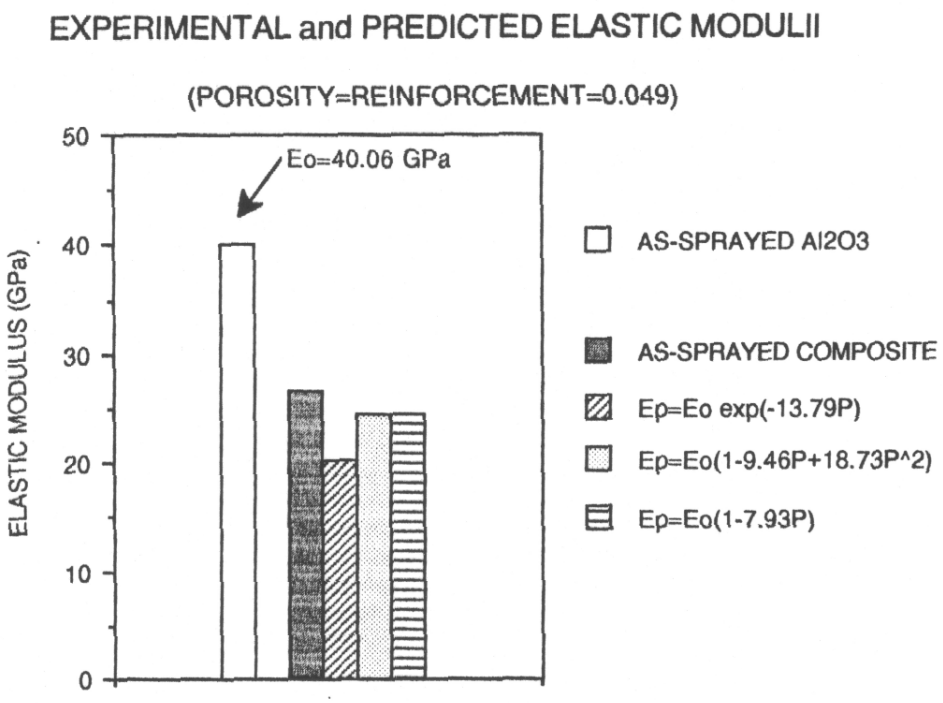
EXPERIMENTAL and PREDICTED ELASTIC MODULII
(POROSITY=REINFORCEMENT=0.049)
ELASTIC MODULUS (GPa)
50
40
30
20
10
0
Eo=40.06 GPa
AS-SPRAYED Al2O3
AS-SPRAYED COMPOSITE
Ep=Eo exp(-13.79P)
Ep=Eo(1-9.46P+18.73P^2)
Ep=Eo(1-7.93P)

TABLE 1

PLASMA-SPRAY PROCESSING PARAMETERS FOR Al_20_3 AND Al_20_3-SiC COMPOSITES

(METCO-3MB SYSTEM)

PARAMETER	VALUE
Arc Voltage	62-65 V
Arc Current	520 A
Primary Gas	Argon
Flow Rate	381 l/min.
Secondary Gas	Hydrogen
Flow Rate	81 l/min.
Powder Carrier Gas	Argon
Flow Rate	71 l/min.
Powder Feed Rate	38 g/min.
Spray Distance	60-80 mm
Traverse Speed	1 m/s

TABLE 2

. PROPERTIES OF PLASMA-SPRAYED Al_20_3

CONDITION	DENSITY (g/cm^3)	FLEXURAL MODULUS (GPa)	STD. DEVIATION	FLEXURAL STRENGTH (MPa)	STD. DEVIATION
As-Sprayed	3.37	40.1	3.6	50.2	3.8
1000 ºC 4 hrs.	3.4	31.5	1.4	43.1	3.3
1300 ºC 1 hr.	3.61	63.8	5	71.4	4.5
1300 ºC 15 hrs.	3.62	75.7	9.6	75.2	8.7
1500 ºC 5 hrs.	3.67	158.3	21.3	121.5	5.8
1600 ºC 9 hrs.	3.7	178.4	30.5	167.9	23.9

TABLE 3

. PROPERTIES OF PLASMA-SPRAYED Al_20_3-3.5 vol % SiC
(30 µm SiC)

CONDITION	DENSITY (g/cm^3)	FLEXURAL MODULUS (GPa)	STD. DEVIATION	FLEXURAL STRENGTH (MPa)	STD. DEVIATION
As-Sprayed	3.4	24.1	3.7	39.5	2.3
1000 ºC 4 hrs.	3.43	43.8	4.4	50.1	3.9
1300 ºC 1 hr.	3.61	80.5	11.2	88.9	6.8
1300 ºC 15 hrs.	3.63	81.2	9.7	90.9	7.2

TABLE 3

. PROPERTIES OF PLASMA-SPRAYED Al_20_3-4.2 vol % SiC
(46 µm SiC)

CONDITION	DENSITY (g/cm^3)	FLEXURAL MODULUS (GPa)	STD. DEVIATION	FLEXURAL STRENGTH (MPa)	STD. DEVIATION
As-Sprayed	3.4	26.5	2.9	42.1	4
1000 ºC 4 hrs.	3.4	39.5	3.5	52.8	3.1
1300 ºC 1 hr.	3.61	75.2	14.9	75.8	13.9
1300 ºC 15 hrs.	3.62	102.4	9.8	99.4	16.6

TABLE 4

. PROPERTIES OF PLASMA-SPRAYED Al_20_3-4.9 vol % SiC
(62 µm SiC)

CONDITION	DENSITY (g/cm^3)	FLEXURAL MODULUS (GPa)	STD. DEVIATION	FLEXURAL STRENGTH (MPa)	STD. DEVIATION
As-Sprayed	3.38	26.7	1.8	39.3	2.1
1000 ºC 4 hrs.	3.43	42.8	3.9	53.7	4.2
1300 ºC 1 hr.	3.63	86.3	6.6	82	8.3
1300 ºC 15 hrs.	3.63	104.9	8.3	86.7	11.5

REFERENCES

1) H. Herman, "Plasma Spray Deposition Processes," MRS Bull., **13** [12] 60-67 (1988).

2) V. H. Wilms, Microstructure of Plasma Sprayed Ceramic Coatings, Ph.D. Dissertation, State University of New York at Stony Brook, 1978.

3) C. E. Holcombe Jr. and G.L. Powell, "Fabrication of Thermally Stable Oxide Coated Crucibles and Thin-Walled Ceramic Articles," Am. Ceram. Soc. Bull., **52** [11] 858 (1973).

4) C. E. Holcombe Jr. , "Fabrication of Thin-Walled Ceramic Structures," Am. Ceram. Soc. Bull., (1978).

5) S. Schindler and W. Schultz, "Plasma Generated Oxide Components,"; pp. 181-191 in 1st Plasma-Technick-Symposium proceedings, vol. 1, Edited by H. Eschnauer, P. Huber, A. R. Nicoll, and S. Sandmeir. Plasma - Technik AG, Wohlen/Switzerland, 1988.

6) D. B. Marshal and J. R. Ritter, "Reliability of Advanced Structural Ceramics - A Review," Am. Ceram. Soc. Bull, **66** [2] 309-17 (1987).

7) P. F. Becher, T. N. Tiegs, J. C. Ogle, and W. H. Warwick, "Toughening of Ceramics by Whisker Reinforcement" ; pp 61-73 in Fracture Mechanics of Ceramics, Vol. 7. Edited by R. C. Bradt, A. G. Evans, D. P. H. Hasselman, and F. F. Lange. Plenum Press, New York, 1986.

17) A.A Cutler, A. C. Hurford, A. V. Virkar, "Pressureless-Sintered A/2OJ-TiC Composites," Mater. Sci and Eng.(1987).

18) G.C. Wei and P.F. Becher, "Development of SiC-Whisker Reinforced Ceramics," Am. Ceram. Soc. Bull., **64** [2] 298-304 (1985).

19) P.F. Becher and G. C. Wei, "Toughening Behavior in SiC-Whisker Reinforced Alumina," J. Am. Ceram. Soc. **67** [12] C267-C269 (1984).

20) A.A. Nicoll, "Protective Coatings and Their Processing," Presented as part of the CEI course on High Temperature Materials and Coatings., June 24-29,1984, Finland.

21) P.A. Siemers, M.A. Jackson, A.L. Mehan, and J.A. Rairden, "Production of Composite Structures by Low Pressure Plasma Deposition," Ceram. Eng. ScL Proc., **6** [7-8] 896-907 (1985).

22) N. Iwamoto, N. Umesaki, S. Endo, and T. Morimura, "Characterization of Plasma Sprayed and Whisker Reinforced Alumina Coatings," J. Mater. ScL, **22** 1113-1119 (1987).

23) C.C. Berndt and J.H. Vi, "The Manufacture and Microstructure of Fiber Reinforced Thermally Sprayed Coatings," Surface and Coatings Technology, **37** 89-110 (1989).

24) C.C. Berndt, "Determination of Material Properties of Ceramic Coatings," Advances in Thermal Spraying, 149-158 (1986).

25) H.D. Steffens and U. Fischer, "Correlation Between Microstructure and Physical Properties of Plasma Sprayed Zirconia," Presented at The National Thermal Spray Conference 1988.

26) P. Boch, D. Fargeot, C. Gault, and F. Platon, "Variations of the Elastic Modulii of Alumina during Structural Phase Transition," Rev. Int. Hautes Temper. et Refract., **18** 85-93 (1981).

27) P.A. Siemers and R.L. Mehan, "Mechanical and Physical Properties of Plasma-Sprayed Stabilized Zirconia," Ceram. Eng. Sci. Proc., **4** [9-10] 828-840 (1983).

28) J.C.K. Wang, The Mechanical Properties of Porous Alumina and Polymer Impregnated Alumina, Ph.D. Dissertation, State University of New York at Stony Brook, 1978.

29) L. Brown, The Dielectric Behavior of Plasma-Sprayed Oxides, Ph.D. Dissertation, State University of New York at Stony Brook, 1987.

30) C.J.P. Steiner, D.P.H. Hasselman, and R.M. Spriggs, "Kinetics of the Gamma-to-Alpha Phase Transformation," J. Am. Ceram. Soc., **54** [8] 412-413 (1971).

31) C.C. Berndt, Personal Communication, Dept. of Materials Engineering, Monash University, Clayton, Victoria, Australia 3168.

32) R.T. Scace and G.A. Slack, "Solubility of Carbon in Silicon and Germanium," J. Chem. Phys., **30** 1551-1555 (1959).

33) R.T. Dolloff, Union Carbide Corp., "Research Study to Determine the Phase Equilibrium Relations of Selected Metal Carbides at High Temperatures," WADD TR 60-143, Contract AF 33(616)-6286 (July, 1960).

34) W.D. Kingery, H.K. Bowen, D.R. Uhlmann, Introduction to Ceramics, John Wiley and Sons, New York 1976

35) H. Herman, "Plasma-Sprayed Coatings," Scientific American **256** [9] 113-117 (1988).

36) E. A. Dean and J. A. Lopez, “Empirical Dependence of Elastic Moduli on Porosity for Ceramic Materials,”J. Am. Ceram. Soc., **66** [5] 366-370 (1983).